Compact cross-sections of mild and high-strength steel hollow-section beams

Pavlovic, Marko; Veljkovic, Milan

DOI
10.1680/jstbu.16.00124

Publication date
2017

Document Version
Accepted author manuscript

Published in
Proceedings of the Institution of Civil Engineers - Structures and Buildings

COMPACT CROSS SECTIONS OF MILD AND HIGH STRENGTH STEEL HOLLOW SECTION BEAMS

Author 1
Dr. Marko Pavlovic, Assistant Professor
- Steel and Composite Structures, Faculty of Civil Engineering and Geosciences (CiTG), Delft University of Technology, Delft, The Netherlands

Author 2
Prof. Milan Veljkovic, Head of Steel and Composite Structures
- Steel and Composite Structures, Faculty of Civil Engineering and Geosciences (CiTG), Delft University of Technology, Delft, The Netherlands

Corresponding author:
m.pavlovic@tudelft.nl; mob: +31 62 417 88 16
Stevinweg 1; 2628 CN; Delft, Nederland

Abstract
The Eurocode 3 rules for the high strength steel (HSS: f_y > 460 MPa) limit the analysis of beams to elastic global analysis and grades up to S700. In order to fully exploit the potential to design lightweight and sustainable steel structures, plastic analysis and the use of higher steel grades with f_y > 700 MPa are desirable. The main concern is the low ultimate-to-yield strength ratio requirement for the high strength steels f_u/f_y > 1.05 according to EN1993-1-12. Its influence on the resistance and rotation capacity of HSS square and rectangular hollow section beams (SHS and RHS) is investigated in this study. The available results of 4-point bending experiments on hollow section beams are validated by FEA with special attention given to imperfections. Parametric study on steel grades S355-S960 indicate that the slenderness limits given in Eurocode 3 need to be reduced both for the mild steels and HSS.

Keywords:
Steel structures; Beams & girders; Codes of practice & standards, High strength steel; Hollow sections; Local stability & ductility

1. Introduction

Improved steel production processes in the past decades opens the possibility for wider application of the higher strength steels, S460 and above, in construction industry. Unfortunately, many rules in EN 1993-1-12 (2010) were adjusted from mild steel for HSS on a very conservative basis. The greatest concern is the limited ductility of the material in terms of lower ultimate-to-yield strength ratio f_u/f_y and the ultimate strain of the material compared to mild strength steels. The design verification according to plastic global and local analysis offered for the steel grades up to S460 in EN 1993-1-1 (2007) provides good opportunity to optimize the

designs. Plastic global analysis with HSS is not allowed according to EN 1993-1-12 (2010) as it is believed not to provide sufficient deformation capacity which would allow redistribution of forces and bending moments in the structure. One of the possibilities to utilize the use of HSS is to design with hollow sections (SHS and RHS) which are being less sensitive to lateral and local instability compared to commonly used open I-shaped cross sections.

Resistance and rotation capacity of hollow section beams depend on strength and the ductility of the material but also on the local buckling influenced by slenderness of the cross section and the imperfections. In EN 1993-1-1 (2007) the slenderness (*b*/*t* ratios) of the cross section parts are limited in order to guarantee the sufficient rotation capacity with regard to local buckling. The European founded project “Rules on High Strength Steels” (RUOSTE, 2016) focuses on research by means of tests and analytical approaches towards removing the most severe obstacles with regard to ductility and stability issues in using HSS, including grades higher than S700.

The slenderness requirement in EN1991-1-1 (2007) does not explicitly relate to the required rotation capacity of the cross section. The ultimate rotation in the plastic hinges φ_{rot} depends on: the type of the structure, e.g continuous beam or frame, span ratios and strain hardening of the material. Stranghöner (1994, 1995) proposed a rotational ductility requirement $R = \varphi_{rot} / \varphi_{pl} - 1 \geq 3$ for hollow sections based on a parametric study of continuous beams.

Results of experiments and FEA published in the recent research on HSS by Wang et al. (2016) show that the cross section classification in EN 1993-1-1 (2007) for the rectangular and square hollow sections (RHS and SHS) are optimistic (unsafe). Wilkinson and Hancock (1997) has shown similar results of the cross section classification for the mild steel, therefore proposed interaction of the flange and web local buckling in function of aspect ratio of the cross-section.

A starting point of investigation shown in this paper is to examine the influence of local imperfections due to forming process and welding of the additional plates to the beams. Therefore experiments are validated by FEA in which imperfections induced by welding of the auxiliary (side) plates for load introduction is considered. In addition, the deformation and residual stresses due to continuous cold forming process are considered in the FE model. In the second step, the influence of imperfections induced by welding and forming process are compared to equivalent geometric imperfections commonly used in the design and research of steel structures. Based on the validated FE modelling, a parametric study on the bending resistance and rotation capacity of hollow section beams is performed for various cross section slendernesses (19-59), steel grades (S355 – S960), and the ultimate-to-yield strength ratio of the material f_u/f_y (1.00 – 1.40).

2. Local buckling in bending experiments

Results of several 3-point bending and 4-point bending experiments in HSS square hollow sections are summarized in Figure 1. The ultimate curvature κ_u, and the curvature corresponding to the plastic bending moment resistance of the cross section κ_{pl} are used to obtain the deformation capacity of the cross section $R = \kappa_u / \kappa_{pl} - 1$, see Figure 1c. This approach is commonly used for the global plastic analysis of structures as it gives information regarding the development of the plastic hinges. The curvature κ is calculated with respect to deflections at the mid-span and the loading points, δ_M and δ_L, in-between the length of the constant bending moment region *a*.

Large scatter of experiment results for resistance and rotation capacity is shown in Stranghöner (1995) and Wilkinson and Hancock (1997) experiments on beams with grade up to S460. Recent results of Zhongcheng and Havula (2015) and Wang et al. (2016), including steel grades up to S700 also show a large scatter, especially of the rotation capacity which can be seen in Figure 1b. A hypothesis analysed here is that reasons for such large scatter are differences in experiment set-ups: primarily in loading details, cross-section properties and beam span (scale). Certainly the level of initial imperfections which depend on the production process and the type of the material (cold-formed, hot-finished, mild steel, high strength steel, etc.) have an influence on the deformation capacity, as well.

Local buckling in 3-point and 4-point bending experiments occurs in the vicinity of the loading point. The loading details shown Figure 2 are designed and optimized for the purpose of the experiment set-ups, all with the aim to minimize the unfavourable impact of the load introduction on the local buckling of the flange. Such loading details are not common in the engineering practice. However, similar influence of welding of the connecting plates in the real joints between steel members can be expected. Wilkinson and Hancock (1997) used a loading detail with welding side plates over the full height of the web. In the Zhongcheng and Havula (2015) experiments side plates are welded only in the bottom half of the web in order to reduce imperfections induced by welding in the compression zone of the hollow section. In Wang et al. (2016) the force is applied by a thick plate placed on the upper flange of the hollow beam in which a timber part is fitted in the region of the applied load.

3. FE model

The finite element model shown in Figure 3 is prepared in ABAQUS (2014) finite element software package with the aim to validate 4-point bending experiments of hollow section beams. Two plane symmetry boundary conditions are used. Experiments on short beam spans between 1.3 m and 1.7 m made of C450 (nominal f_y = 450 MPa), were performed by Wilkinson and Hancock (1997). Long span beams made of S700 with spans from 3 m to 6.8 m were performed by Zhongcheng and Havula (2015). For both experiments cold-formed hollow sections were produced in a continuous forming (CF) process shown in Figure 4a. In total seven cases are analysed covering a wide range of cross-section dimensions, thicknesses and aspect ratios.

Table 2 summarizes the cases considered in the validation analysis with details describing the assignment of imperfections induced by welding in FEA.

Experiments are modelled using shell elements S3D4R for the beam and solid elements C3D8R for loading plates and welds with proper coupling by the tie constraint surface pairs, see detail views in Figure 3. Due attention is given to properly model the geometry of welded details in each experiment according to Figure 2(a and d). Exact material properties obtained in tensile tests on coupons that are cut from the flange, web and the corner region of each specimen are considered in FEA. Analysis is performed with displacement control load by using the General/Static solver with stabilization, implemented in ABAQUS (2014).

4. Influence of the imperfections

Rectangular and square hollow section beams are produced in the direct and continuous forming processes, as shown in see Figure 4a, resulting in bow-out imperfections and residual stresses as illustrated in Figure 4b. In addition, welding of the auxiliary members/plates to the walls of hollow sections introduces additional imperfections.

The complex combination of the material and geometric imperfections are often presented by the most unfavourable equivalent geometric imperfection in state-of-the-art FEA. The form is taken as a sinusoidal shape along the beam obtained as the shape of the critical eigen-mode in linear buckling analysis, e.g. due to bending loading as shown in Figure 4c. However, measurements of imperfections on mild steel and high strength steel hollow section beams in RUOSTE (2016), Wilkinson and Hancock (1997), Wang et al. (2016) and Ma et al. (2015a) show that a “bow-out” imperfection, constant along the length of the beam is dominant. A wide range of the amplitudes of the bow-out imperfection, between 1/100 – 1/1300 is measured as shown in Table 1. None of the research succeeded to establish an distinctive rule between the amplitude of the imperfection and steel grade or slenderness, neither to validate experiment results by imposing measured bow-out imperfections in FEA. Wilkinson and Hancock (1999) found large variation of amplitude and wave length of the equivalent sinusoidal shape imperfection in FEA that is needed to validate variety of 4-point bending experiments. Wang et al. (2016) reported that an imperfection amplitude of $t/50$ in the FEA best fits the results from experiments. These imperfections are much lower than the amplitude of the local equivalent imperfection c / 200 according to EN 1993-1-5 (2006), where c is the equivalent width of the part of the cross-section in compression. So far, there are no clear recommendations on how to consider basic variables concerning equivalent geometric imperfections in the research and detailed design verifications, except the quite rough and conservative values given in EN 1993-1-5 (2006) for FEA assisted design of steel structures.

4.1. Deformation and residual stresses induced by welding

Welding of steel plates causes local deformations of the cross-section and residual stresses in the heat affected zone (HAZ). Angular distortion, called here the transverse bending (TB) after

Jang et al. (2002), is shown in Figure 5a. as the most important in the case of imperfections imposed by the welds on the web or the flange of the hollow section beam. Level of the angular distortion depends on various parameters, such as: size of the weld and welding technique which influence the heat input, thickness of the plate, etc. Jang et al. (2002), and Wang et al. (2009), have combined experiments and thermo-elastic-plastic (TEP) analysis of bead-on-plate and T-joint fillet welds. Results of their analysis are shown in Figure 5b and c where the angular distortion is presented in function of the relative heat input, i.e. heat input energy vs. thickness of the plate. It is noticed that the angular distortion has a limiting value of TB_{lim} = 0.022 rad, which is conservatively used in the analysis shown here.

Prediction of the imperfections induced by welding in hollow section beams is modelled by the simplified inherent strain method (ISM) capable of analysing large structural components. Residual strains due to welding are applied as predefined strain field in HAZ, as shown in Figure 6a, resulting in residual stresses and deformation around the weld, see Figure 6b and c, respectively. Therefore, the need of demanding TEP analysis on complex and large-scale geometry is excluded. The distribution of induced strains in fillet welds to be used in ISM is not clearly defined in available literature. TEP analysis is performed on plain strain 2D model of the longitudinal section in the middle of the height of the weld, see detail in Figure 6c. Abaqus Welding Interface (AWI, 2015) is used to define the parameters of the TEP analysis. The aim was to obtain the realistic and feasible model of distribution of the plastic strains perpendicular to the weld path producing the angular distortion in the HAZ and weld, as the input for ISM. Results of TEP analysis are presented in Figure 7a where the plastic strains after the weld cooling are shown as contour plot and in section cuts. Section cut A-A is defined through thickness of the web plate and the web and section B-B is at the interface between the web and the weld. Idealised distribution of those plastic strains in cross sections A-A and B-B are assumed, as shown in Figure 7a and illustrated in Figure 7b. Constant value of the plastic strain in the weld ε_{w} at the outer surface of the web and linear reduction to zero strain at the internal surface are assumed. The effective width of the HAZ on the web $b_{\text{w,eff}}$ is estimated to 1.5 of the weld width, as shown in Figure 7a and b and formula Eq. (1), where a_{w} is the weld throat thickness. For the prescribed value of the angular distortion *TB*, shown in Figure 7c, the strain ε_{w} is calculated based on the shrinkage Δ and the effective width $b_{\text{w,eff}}$ at the outer surface, as given in Eq. (2).

$$b_{\text{w,eff}} = 1.5 a_{\text{w}} \sqrt{2}$$

1.

$$\varepsilon_{\text{w}} = TB \cdot t / b_{\text{w,eff}}$$

2.

Based on the effective width $b_{w,eff}$ and the strain level ε_w calculated in Table 2 the welding induced imperfections are imposed in a load free calculation step which is used to obtain the equilibrium of the applied predefined field of strains. Predefined strains are applied to the 4-point bending FE model as temperature strains in the weld and portion of the web having width equal to $b_{w,eff}$ and height equal to the length of the weld, see Figure 6a. Uniform temperature (strain) distribution equal to ε_w is applied to the weld. Welding deformations in longitudinal weld direction are negligible for the phenomena analysed in this study. Therefore, strains induced by welding are applied only in transverse weld direction. Orthotropic expansion properties for the solid weld part and affected portion of the web modelled with shell elements are applied as: $\alpha_{11} = 1$, $\alpha_{22} = 0$, $\alpha_{33} = 1$, with "11" denoting the longitudinal direction of the beam, see Figure 6a. Strain (temperature) distribution in affected portion of the web is applied as predefined field linearly varying through the thickness of the shell elements.

Figure 8 shows detailed presentation of the obtained deformation in the longitudinal section of the web, see Figure 6c, i.e. at the height where the maximum out of plane welding induced deformation of the web is obtained. Deformations caused by welding of each case are given in Table 2 as outward and inward deformations of the web δ_{out} and δ_{in}, respectively. Almost equal amplitude of the absolute deformation of the web $(\delta_{out} - \delta_{in}) \approx d / 350$ is obtained in all analysed cases. The angular distortion is calculated in each case by differentiate of the out of plane web deformation. In average, 70% of the prescribed angular distortion $TB = 0.022$ rad is obtained. This is the consequence of restraint provided by hollow section flanges in 3D model of the cross-section.

4.2. Influence of the forming process

The residual deformations (see Table 1, Figure 4a,b) and residual stresses that depend on the forming process (direct or continuous), steel grade and slenderness might also affect the local buckling behaviour of the hollow section beam. In RUOSTE projects (2016) and papers published by researchers: Li et al. (2009), Tong et al. (2012), Sun and Packer (2014), Ma et al. (2015b) almost zero membrane residual stresses were measured. However, significant bending residual stresses, between 50% and 90% of the yield strength, are measured in longitudinal and transverse direction of the hollow section beam.

Bending residual stresses and deformations are indirectly applied in FEA by imposing predefined strains in the same manner as the imperfections induced by welding are applied. The orthotropic expansion properties are defined as: $\alpha_{11} = 1$, $\alpha_{22} = -1$ in order to apply opposite sign of the bending residual stresses in the longitudinal and transverse direction as obtained in the experiments. The amplitudes of applied strains are -0.0023 and +0.0023 at the outer and

inner face of the shell elements, respectively, in order to achieve approximately 70% of the nominal yield strength and elastic modulus equal to f_y = 700 MPa and E = 210,000 N/mm^2.

4.3. Comparison of the results

The FEA results are compared to Wilkinson and Hancock (1997) experiments on short span mild steel beams and Zhongcheng and Havula (2015) experiments on long span HSS in Table 3 and Table 4, respectively. Two characteristic cases of both sets of experiments are presented in Figure 9. The FEA results are obtained considering different initial states of imperfections:

a) without any imperfections (FEA,no),

b) with imperfections induced by welding (FEA,w),

c) with imperfections induced by forming process (FEA,f) and

d) with imperfections induced by welding and forming process (FEA,w+f).

Ultimate resistance is well predicted by FEA regardless the initial state of imperfections. However, without considering imperfections the deformation capacity is overestimated up to 46 % in average, see Table 3 and Table 4. Applying only the imperfections induced by welding (FEA,w) gives very good results in terms of prediction of the deformation capacity in all the cases analysed. In addition, the failure mode, local buckling near the loading plates, see Figure 2(d and e) is well predicted in FEA. If only the imperfections induced by the forming process are applied (FEA,f), the obtained deformation capacities are overestimated up to 28 % in average. The best agreement between the experiment and FEA results, 2-4% difference, is obtained if only the deformations and residual stresses induced by welding (FEA,w) are applied. If both the imperfections induced by welding and the forming process are applied (FEA,w+f) the obtained deformation capacity is increased compared to the case where only welding induced imperfections are applied, leading to an average overestimate of 22 %. The reason for such unexpected behaviour is explained through comparison of initial deformations due to the welding and the forming process and the deformation of the cross section at the post-buckling stage in the cross section where the local buckling occurs. Figure 10 shows that the inward deformation of the flange is induced by outward deformation of the web in the case of welding. This which matches to the final buckled shape of the critical cross section. The forming process induces the outward deformation of the flange, which is opposite to the final buckled shape of the critical cross section, therefore having favourable influence and increasing the deformation capacity. However in most of the cases the deformation capacity is decreased in case of applying imperfections induced by the forming process due to the interaction of the web and the flange buckling under bending loading. Flange buckling is dominant in the case of square sections while the influence of the web buckling increases with increase of the relative height of the cross section, see Wilkinson and Hancock (1997). In both cases of the welding and the forming process induced imperfections the outward deformation of the web is produced which matches the final buckled shape, thus decreasing the deformation capacity. The interaction of favourable and unfavourable influence at the flange and web buckling leads to reduced deformation capacity compared to cases where no imperfection is applied in analysis. When the

welding and forming process induced imperfections are combined, the favourable influence of the forming induced imperfections at the flange reduces the unfavourable influence of the welding induced imperfections leading to previously noticed unexpected superposition of the two imperfections. It is concluded that the influence of the imperfections induced by the forming process have negligible, and in some cases, un-conservative effects on local buckling behaviour of hollow section beams.

4.4. Equivalent geometric imperfections

Influence of geometric imperfections in form of the eigen-mode and bow-out imperfections, see Figure 4, are analysed to show their influence on the scatter of rotation capacity obtained in experiments in comparison to imperfections induced by welding. Square hollow sections considered in long-span experiments Zhongcheng and Havula (2015) and nominal material properties of S500, S700 and S960 materials are used, see Table 5 and section 5.1. Two sets of imperfection amplitudes are analysed:

a) 1/700 – equivalent to the amplitude of the imperfections induced by welding and average value obtained in measurements, see Table 2 and Table 1, respectively;
b) 1/200 – according to EN 1993-1-5 (2006) recommendation.

Results with different initial states in FEA are compared in Figure 11. Large scatter of 0.1 and 3 (non-dimensional) for the bending resistance and the rotation capacity is obtained, respectively. Even larger scatter can be observed in experiments, see Figure 1. Higher resistance and rotation capacity is obtained with bow-out imperfections with amplitude 1/200, compared to the imperfections induced by welding having an lower equivalent amplitude 1/700. This confirms the previous observation about dominant influence of the welding induced imperfections. Therefore, the higher ductility can be expected for the hollow section beams without plates welded to it. Approximately 2% lower bending resistance and 30% lower rotation capacity is obtained with equivalent eigen-mode imperfections, compared to the imperfections induced by the welding, both having amplitudes of 1/700. This is due to the fact that with the equivalent eigen-mode imperfections the correct failure mode, buckling near the loading plates, is not obtained. Applying the eigen-mode equivalent geometric imperfection with amplitude 1/200, as recommended according to EN 1995-1-5 (2006), results in approximately 4% and 60% reduced bending resistance and rotation capacity, respectively. This recommendation gives very conservative results of the rotation capacity. Therefore an pragmatic approach is used in parametric FEA by applying the welding induced imperfections only as those best-fit the experiment results and more importantly properly describe the failure mode in the standardized test set-up.

5. Parametric study of HSS and MS hollow section beams resistance and deformation capacity

Parametric study of the rotation capacity and bending resistance of SHS and RHS beams (see Table 5) is performed in order to establish cross section classification parameters for HSS and to compare them to the mild steel beams.

Parametric study is performed using previously validated 4-point bending test set-up, with span 5.8 m beam and the length of the constant bending moment region of $L/3$ = 1932 mm. Flange and web slenderness is varied in the range 16 to 115 in order to check validity of the cross-section class limits according to the EN 1993-1-1 (2007).

5.1. Materials

Series of 14 coupon tests of mild-steels and high-strength steels of Scandinavian producers are shown in Figure 12. Generally, the curves are divided into two groups:

1) materials having yielding plateau which is the characteristic for the mild-steels;

2) materials having onset of plasticity prior to the yield strength which is characteristic for the high-strength steels.

For the parametric study, the two sets of materials are defined using generic stress-strain curves having two linear and two parabolic parts, see Figure 13. The elastic behaviour and the initial plastic behaviour: the yielding plateau and onset of plasticity in case of MS and HSS, respectively, are described by two linear parts. The strain hardening and softening parts of the stress-strain curve are defined by the two parabolic segments, having horizontal tangents at the ultimate strength.

Nominal materials with minimum requirements of EN 1993-1-1 (f_u/f_y = 1.1; A_g = 15ε_y; A_5 = 15%) and EN 1993-1-12 (f_u/f_y = 1.05; A_g = 15ε_y; A_5 = 10%) are analysed for the MS and HSS, respectively. It is assumed that the systematic variation of the material properties will indicate requirements of the nominal criterions. For the MS the minimum design code requirements are compared to the results obtained by idealised generic stress-strain curves corresponding to the real materials, having much higher ultimate-to-yield strength ratios up to f_u/f_y = 1.4, see Figure 13. In the case of HSS, the nominal materials conforming to the design code requirements are compared to the possible increases and decreases of ultimate-to-yield strength ratio in range f_u/f_y = 1.0 – 1.3, see Table 6. The onset of plasticity in case of HSS is defined as a function of the yield strength see Eq. 3 (RUOSTE, 2016). This definition is based on analysis of the stress-strain curves shown in Figure 12.

$$\Omega_p = R_{p0.01} / R_{p0.2} = 1.1 - 0.1 R_{p0.2} / 235 \leq 1.0 \quad (R_{p0.2} \text{ in MPa})$$

3.

5.2. Slenderness limits for Mild steel beams

Considering rotation capacity criterion $R > 3$ defined in Stranghöner (1995) and currently used in the Eurocodes and the resistance criterion $M_u/M_{pl} > 1$, cross section class 1 and class 2 flange slenderness limits are obtained, respectively. Results are shown in Table 7 shown and Figure 14.

If idealised properties of realistic mild steel material are considered class 1 limit $c/(t\varepsilon) < 33$ is nearly satisfied for S355 but lower limit $c/(t\varepsilon) < 29.7$ is obtained for S460, see Figure 14b. This complies with findings of Taras et al. (2013) proposing reduction of current class 1 slenderness limit of internal cross section parts to $c/(t\varepsilon) < 28$. Flange slenderness limit 38 for section class 2 is satisfied for both steel grades.

Considering nominal material properties according to minimum EN 1993-1-1 (2007) requirements (results given by solid lines in Figure 14), the rotation capacity and section class 1 limit are not significantly affected compared to the results obtained by considering idealised properties of realistic mild steel material. However, lower limit for section class 2 is obtained: $c/(t\varepsilon) < 31$. This limit is independent of the steel grade analysed. The result is much lower compared to EN 1993-1-1 (2007) limit which is $c/(t\varepsilon) < 38$ and reduced section class 2 limit $c/(t\varepsilon) < 34$ proposed by Taras et al. (2013). Similar reduction of those limits is confirmed by Wang et al. (2016). Reason for such low class 2 limit is use of the nominal material properties which are much lower compared to realistic material properties in case of mild steels.

5.3. Slenderness limits for High Strength steel beams

5.3.1. Influence of the ultimate-to-yield strength ratio

Section class 1 and class 2 flange slenderness limits for HSS square hollow sections shown in Figure 15 are determined following the rotation requirement $R > 3$ and resistance $M_u/M_p| > 1$ criteria. Both criterions lead to the nonlinear dependence with regard to the ultimate-to-yield strength ratio f_u/f_y. The curves representing the class 1 criterion clearly justifies “the minimum hardening requirement” i.e. $f_u/f_y \geq 1.05$ according to the EN 1993-1-12 (2010) as an significant change in the slenderness requirement is noticed at this limit. No significant influence of the steel grade to the class 2 limit is obtained but higher influence on the rotation capacity is noticed.

Considering the minimum EN 1993-1-12 (2010) requirement for the ultimate-to-yield strength ratio $f_u/f_y \geq 1.05$, class 1 and class 2 flange slenderness limits $c/(t\varepsilon)$ are 30 and 35, respectively. The conclusion is that the limits for HSS are higher compared to the limits for mild steels if the minimum design code requirements of the material are considered. However, in order to achieve the section class 1 and class 2 the flange slenderness limits of 33 and 38, according requirements EN 1993-1-1 (2007), respectively, the minimum ultimate-to-yield strength ratio of

the HSS material are 1.30 and 1.10. The limit for the cross section class 1 of $f_u/f_y \geq 1.3$ is imposed by the rotation capacity requirement $R \geq 3$, see Figure 15b. The rotation requirement of $R \geq 3$ in the analysed cases corresponds to plastic rotation of the plastic hinge in range from $\varphi_{rot} = 4°$ to $\varphi_{rot} = 13°$, depending on the height of the cross section and the steel grade. This requirement is hardly expected to be achieved by HSS. However, for each specific structure, the plastic global analysis can be performed in order to obtain if the lower value of the rotation capacity R is sufficient for forming of the mechanism. Finally, the cross section class 2 is achievable by the higher strength stills leaving the opportunity for the plastic analysis at level of the cross section.

6. Conclusions

Welding of the connecting plates at the cross section where the concentrated forces are applied has strong influence on geometric imperfections. FEA validation of series of 4-point bending experiment results clearly showed the dominating influence of imperfections (residual stresses and deformations) induced by welding compared to the influence of imperfections induced by forming process. Welding the connecting plates for the joining details to RHS and SHS sections, reduces its resistance and deformation capacity in bending approximately 5 % and 20 %, respectively. The values have been calculated for the optimized welded joint detail in 4-point bending experiment which produces low amount of imperfections in the compression zone. The knowledge gained from analysing the influence of generic welded joint details in 4-point bending experiments is transferable to the design of engineering steel structures. Attention should be given to details with worse imperfections in the compression zone which are likely to need lower slenderness limits to attain the same plastic rotations. Higher ductility can be expected for the hollow section beams without plates welded to it.

Cross section class limits for hollow sections are obtained from results of FE parametric study in 4-point bending test set-up, considering strength and rotation requirement of $M_u/M_{pl} \geq 1$ and $R = \varphi_{rot} / \varphi_{pl} - 1 \geq 3$, respectively. For the mild steel beams following are the main conclusions:

1. If the realistic material properties of mild steel are considered, the flange slenderness limits given in EC3 for class 1 and class 2, (33 and 38, respectively), are sufficient for S355 but lower cross-section class 1 limit $c/(t\varepsilon) < 29$ is obtained for S460.
2. Considering nominal material properties according to minimum EN 1993-1-1 (2007) requirements, ($f_u/f_y = 1.1$), the rotation capacity is not significantly affected compared to realistic materials. However, a lower section class 2 flange slenderness limit 31 is obtained.

Influence of the higher steel grades on the hollow section class limits are analysed and it is found that the ultimate-to-yield strength ratio has rather stronger influence on resistance and rotation capacity:

3. Considering the minimum requirement of EN 1993-1-12 (2010) for the ultimate-to-yield strength ratio $f_u/f_y = 1.05$, class 1 and class 2 flange slenderness limits 30 and 35, respectively, are obtained. The limits obtained for HSS are lower than the limits required by the EN 1993-1-1 (2007) but higher compared to the limits obtained for nominal properties of the mild steels.
4. In order to achieve the section class 1 and class 2 flange slenderness limits given in EN 1993-1-1 (2007), the minimum required ultimate-to-yield strength ratio of the HSS material are $f_u/f_y > 1.30$ and $f_u/f_y > 1.10$, respectively.

References

ABAQUS (2014). User Manual, Version 6.13 Analysis User's Guide, 3DS Simulia.

AWI (Abaqus Welding Interface) (2015). ABAQUS Extensions, 3DS Simulia.

EN 1993-1-1 (2007). Design of steel structures, Part 1-1: General rules and rules for buildings, Brussels, Belgium: European Committee for Standardization.

EN 1993-1-5 (2006). Design of steel structures, Part 1-5: Plated structural elements, Brussels, Belgium: European Committee for Standardization.

EN 1993-1-12 (2010). Design of steel structures, Part 1-12: Additional rules for the extension of EN 1993 up to steel grades S700, Brussels, Belgium: European Committee for Standardization.

Jang CD, Lee CH and Ko DE (2002) Prediction of welding deformations of stiffened panels, Proc Instn Mech Engrs Vol 216 PartM: J Engineering for the Maritime Environment p133-143.

Li SH, Zeng G, Ma YF, et al. (2009) Residual stresses in roll-formed square hollow sections, Thin-Walled Structures 47 p505-513.

Ma JL, Chan TM and Young B (2015a) Experimental Investigation on Stub-Column Behavior of Cold-Formed High-Strength Steel Hollow section Sections., Journal of Structural Engineering ASCE.

Ma JL, Chan TM and Young B (2015b) Material properties and residual stresses of cold-formed high strength steel hollow sections, Journal of Constructional Steel Research 109 p152-165.

RUOSTE (2016). RUOSTE Project (Rules On High Strength Steel) RFSR-CT-2012-00036 - Final Report (in press). Research Found For Coal and Steel.

Ruukki (2011). Steel sections - Hollow sections - Dimensions and cross-sectional properties. Rautaruukki Corporation.

Sedlacek G et al. (1995) Investigation of the rotation behaviour of hollow section beams, ECSC, Technical report EUR 17994 EN.

Sun M, Packer JA (2014) Direct-formed and continuous-formed rectangular hollow sections, Journal of Constructional Steel Research 92 p67-78.

Stranghöner N, Sedlacek G (1994) Rotation requirement and rotation capacity of rectangular, square and circular hollow section beams, in Grundy P, Holgate A and Wong B edition,

Proceedings Sixth International Symposium on Hollow section Structures, Melbourne, Australia 14-16 December p143-150.

Stranghöner N (1995) Untersuchungen zum Rotationverhalten von Trägern aus Hohlprofilen, PhD thesis (in German), title in English „Investigation of the Rotation Behaviour of Hollow Section Beams“, RWTH Aachen.

Taras A, Greiner R and Unterweger H (2013). Proposal for amended rules for member buckling and semi-compact cross-section design, Technical Report, Consolidated Version of Documents of the Same Title Submitted to the SC3 Evolution Group 1993–1-1, Paris.

Tong L, Hou G, Chen Y, et al. (2012) Experimental investigation on longitudinal residual stresses for cold-formed thick-walled square hollow sections, Journal of Constructional Steel Research 73 p105-116.

Wang R, Zhang J, Serizawa H and Murakawa H (2009) Study of welding inherent deformations in thin plates based on finite element analysis using interactive substructure method, Materials and Design 30 p3274-3481.

Wang J, Afshan S, Gkantou M, et al. (2016) Flexural behaviour of hot-finished high strength steel square and rectangular hollow sections, Journal of Construction al Steel Research 121 p97-109.

Wilkinson T and Hancock J (1997). Tests for the compact web slenderness of cold-formed rectangular hollow sections, Research Report R744, The University of Sydney.

Wilkinson T and Hancock G (1999). Finite element analysis of plastic bending of cold-formed rectangular hollow section beams, Research Report R792, The University of Sydney.

Zhongcheng M and Havula J (2015). Bending tests of S700 tubes, Report 2015-56, University of Applied Sciences HAMK, HAMK, Hameenlinna, Finland.

Figure captions (images as individual files separate to your MS Word text file).

Figure 1. Experiment results of rectangular and square hollow section beams: a) non-dimensional bending resistance ; b) rotation capacity; c) typical non-dimensional moment-rotation curves.

Figure 2. Local web and flange buckling near the loading section in bending experiments and FEA: a) Wilkinson and Hancock; b) Stranghöner; c) Wang et al.; d) Zhongcheng and Havula; e) FEA validation

Figure 3. FE model of 4-point bending experiments: a) Forming processes (Li et al. 2009); b) “bow-out” imperfections; c) Eigen-mode due to bending load.

Figure 4. Typical equivalent geometric imperfections used in nonlinear FEA: a Shape of distortion; b) bead-on-plate welds, Jang et al. (2002); c) fillet welds, Wang et al. (2009).

Figure 5: Transverse bending (angular distortion) due to welding: a) applied strains; b) residual stresses (von Mises); c) out of plane deformations.

Figure 6. Welding induced imperfections applied in FE model of RHS 140x140x6.

Figure 7. Model of distribution of plastic strains induced by welding: a) TEP analysis of fillet weld between the web and the loading plate; b) plastic strain distribution: c) strain vs. angular distortion TB.
Figure 8. Out of plane deformation of the web in RHS 140x140x6: a) the deformed shape (scale x20); b) the deformation and c) the first derivative of the displacement (angular distortion)
Figure 9. Validation of imperfections in FEA vs. experiment results: a) RHS 150x50x4 - Wilkinson and Hancock (1997); b) SHS 150x150x8 - Zhongcheng and Havula (2015).
Figure 10. Diminishing effect of the forming induced imperfections on reduction of the rotation capacity.
Figure 11. Influence of equivalent geometric imperfections vs. welding induced imperfections on cross section classification: a) Non-dimensional bending resistance; b) Rotation capacity .
Figure 12. Results of tensile tests on various HSS and MS (RUOSTE, 2016).
Figure 13. Materials used in the parametric study: a) Mild-steel (MS); b) High-strength steel (HSS).
Figure 14. Cross section class 1 and 2 limits for mild-steel beams - realistic vs. nominal material: a) Non-dimensional moment; b) Rotation capacity.
Figure 15. Cross section class limits for high strength steel beams – influence of the ultimate-to-yield strength ratio: a) Resistance criterion – Class 2; b) Rotation capacity criterion – Class 1.

Table captions

Table 1. Bow-out imperfections in hollow section beams and stub columns due to the forming process
Table 2. Cases considered in the experiments vs. FEA validation and application of the imperfections induced by welding in the FE models
Table 3: Results of 4-point bending FEA vs. Wilkinson and Hancock (1997) experiments
Table 4. : Results of 4-point bending FEA vs. Zhongcheng and Havula (2015) experiments
Table 5. Hollow sections considered in the parametric study
Table 6. Materials used in the parametric study
Table 7. class 1 and class 2 flange slenderness limits for mild steel hollow section

Notation and abbreviations list

a length of the constant bending moment region in the 4-point bending test;
a_w thickness of the weld throat;
b width of the wall of the hollow cross section;
$b_{w,eff}$ the effective width of the heat affected zone on the web to which the inherent strains area applied;
c effective width of the plate representing the wall of the hollow cross section excluding corners;
t thickness of the wall of the hollow cross section;
L span of the beam in the 4-point bending test;

R	deformation capacity of the cross section / rotation requirement;
f_y	yield strength of the steel material;
f_u	ultimate strength of the steel material;
ε_w	the inherent strain due to welding;
δ_M	deflections at the mid-span in the 4-point bending test;
δ_L	deflections at the loading points in the 4-point bending test;
φ_{rot}	ultimate rotation in the plastic hinges;
φ_{pl}	rotation in the plastic hinge corresponding to the plastic bending moment resistance of the cross section;
κ_u	ultimate curvature;
κ_{pl}	curvature corresponding to the plastic bending moment resistance of the cross section;
HSS	High Strength Steel;
FEA	Finite Element Analysis;
RHS	Rectangular Hollow Section;
SHS	Square Hollow Section;
ISM	Inherent Strain Method;
TEP	thermo-elastic-plastic analysis;
HAZ	heat affected zone;
TB	transverse bending.

Table 1: Bow-out imperfections in hollow section beams and stub columns due to the forming process

Reference	Steel grade	Cross section dimens. b, d (mm)	Thicknesses t (mm)	No. of spec. (-)	Max. imperf. (-)	Min. imperf. (-)	Average (-)
RUOSTE (2016a)	S700, S960	110 – 200	3 - 7	9	1/110	1/520	1/235
Wilkinson and Hancock (1997)	C350, C450	75 – 150	2 – 5	-	-	-	1/500
Wang et al. (2016)	S460, S690	50 – 100	4 – 6.3	11	1/320	1/1300	1/900
Ma et al. (2015)	S690, S690	80 – 160	4	5	1/250	1/740	1/420

Table 2: Cases considered in the experiments vs. FEA validation and application of the imperfections induced by welding in the FE models

Profile	Steel grade	Yield strength	Weld throat thickness	Weld height	Eff. width of transv.strains	Welding induced strain	Relative def. of the web		Obtained ang. distort.
d x b x t (mm)		f_y; $R_{p.02}$(MPa)	a_w (mm)		$b_{w,eff}$ (mm)	e_w (-)	d / δ_{out}	d / (δ_{out} - δ_{in})	TB (rad)
RHS 100x50x2	C450	449	3	full	6.4	0.007	417	385	0.015
SHS 100x100x3	C450	445	3	full	6.4	0.010	400	345	0.015
RHS 150x50x4	C450	457	3	full	6.4	0.014	428	333	0.020
RHS 150x100x4	S700	743	3	half	6.4	0.014	517	395	0.017
SHS 140x140x6	S700	766	4.5	half	9.6	0.014	681	368	0.015
SHS 150x150x6	S700	767	4.5	half	9.6	0.014	600	357	0.016
SHS 150x150x8	S700	725	6	half	12.7	0.014	1000	357	0.015

Table 3: Results of 4-point bending FEA vs. Wilkinson and Hancock (1997) experiments

Profile	Non-dimensional bending moment			Non-dimensional curvature								
	Exp.	FEA with weld. ind. imperf.	FEA vs. Exp.	Exp.	FEA (different initial states)				FEA vs. Experiment			
					No imperf.	Weld. ind. imperf.	Forming ind. Imp.	Welding + Form.				
d x b x t (mm)	$\frac{M_{u,Exp}}{M_{pl}}$	$\frac{M_{u,FEA,w}}{M_{pl}}$	$\frac{M_{u,FEA,w}}{M_{u,Exp}}$	$\frac{\kappa_{u,Exp}}{\kappa_{pl}}$	$\frac{\kappa_{u,FEA,no}}{\kappa_{pl}}$	$\frac{\kappa_{u,FEA,w}}{\kappa_{pl}}$	$\frac{\kappa_{u,FEA,f}}{\kappa_{pl}}$	$\frac{\kappa_{u,FEA,w+f}}{\kappa_{pl}}$	$\frac{\kappa_{u,FEA,no}}{\kappa_{u,Exp}}$	$\frac{\kappa_{u,FEA,w}}{\kappa_{u,Exp}}$	$\frac{\kappa_{u,FEA,f}}{\kappa_{u,Exp}}$	$\frac{\kappa_{u,FEA,w+f}}{\kappa_{u,Exp}}$
100x50x2	1.13	1.11	0.98	2.65	4.9	3.05	3.6	3.45	1.85	1.15	1.36	1.30
100x100x3	1.04	1.04	1.00	1.75	2.15	1.6	2.12	2.05	1.23	0.91	1.21	1.17
150x50x4	1.23	1.22	0.99	8	10.4	8.5	10.1	9.5	1.30	1.06	1.26	1.19
Average			0.99						1.46	1.04	1.28	1.22

Table 4: Results 4-point bending FEA vs. Zhongcheng and Havula (2015) experiments

Profile	Ultimate load			Mid-span deflection at ultimate load								
	Exp.	FEA with weld. ind. imperf.	FEA vs. Exp.	Exp.	FEA (different initial states)				FEA vs. Experiment			
					No imperf.	Weld. ind. imperf.	Forming ind. imp.	Welding + Form.				
d x b x t (mm)	$F_{u,Exp}$ (kN)	$F_{u,FEA,w}$ (kN)	$\frac{F_{u,FEA,w}}{F_{u,EXP}}$	$\delta_{u,Exp}$ (mm)	$\delta_{u,FEA,no}$ (mm)	$\delta_{u,FEA,w}$ (mm)	$\delta_{u,FEA,f}$ (mm)	$\delta_{u,FEA,w+f}$ (mm)	$\frac{\delta_{u,FEA,no}}{\delta_{u,Exp}}$	$\frac{\delta_{u,FEA,w}}{\delta_{u,Exp}}$	$\frac{\delta_{u,FEA,f}}{\delta_{u,Exp}}$	$\frac{\delta_{u,FEA,w+f}}{\delta_{u,Exp}}$
150x100x4	156	155	0.99	111	137	118	128	123	1.23	1.06	1.15	1.11
140x140x6	131	129	0.98	471	538	455	524	480	1.14	0.97	1.11	1.02
150x150x6	148	145	0.98	388	419	367	418	390	1.08	0.95	1.08	1.01
150x150x8	197	194	0.98	630	855	705	856	748	1.36	1.12	1.36	1.19
Average			0.99						1.20	1.02	1.18	1.08

Table 5: Hollow sections considered in the parametric study

Section shape (aspect ratio)	Height	Width	Thick.	Web slenderness $(d\text{-}3t)/t\varepsilon$ (-)					Flange slenderness $(b\text{-}3t)/t\varepsilon$ (-)				
	d (mm)	b (mm)	t (mm)	S355	S460	S500	*S700*	S960	S355	S460	S500	*S700*	S960
SHS *d*/*b*=1.0	160	160	10	16.0	18.2	19.0	22.4	26.3	16.0	18.2	19.0	22.4	26.3
	150	150	8	19.4	22.0	23.0	27.2	31.8	19.4	22.0	23.0	27.2	31.8
	140	140	6	25.0	28.4	29.7	35.1	41.1	25.0	28.4	29.7	35.1	41.1
	150	150	6	27.0	30.8	32.1	38.0	44.5	27.0	30.8	32.1	38.0	44.5
	160	160	5	35.6	40.6	42.3	50.1	58.6	35.6	40.6	42.3	50.1	58.6
RHS *d*/*b*=1.5	150	100	6			32.1	38.0	44.5			19.9	23.6	27.6
	180	120	6			39.4	46.6	54.6			24.8	29.3	34.4
	180	120	5			48.1	57.0	66.7			30.6	36.2	42.4
	180	120	4			61.3	72.5	84.9			39.4	46.6	54.6
	240	160	5			65.6	77.7	91.0			42.3	50.1	58.6
RHS *d*/*b*=2.0	200	100	6			44.2	52.4	61.3			19.9	23.6	27.6
	200	100	5			54.0	63.9	74.8			24.8	29.3	34.4
	240	120	5			65.6	77.7	91.0			30.6	36.2	42.4
	240	120	4			83.1	98.4	115.2			39.4	46.6	54.6

Table 6: Materials used in the parametric study

Steel grade	Yield strength f_y (MPa)	Ultimate-to-yield strength ratio f_u/f_y (-)	Uniform elongation *A*g (%)	Fracture strain A_5 (%)
S355	355	1.10	2.5	15
S460	460	1.10	3.3	15
S355	355	1.40	15	30
S460	460	1.25	10	20
S500	500	1.0, 1.025, 1.05, 1.1, 1.2, 1.3	3.6	10
S700	700	1.0, 1.025, 1.05, 1.1, 1.2, 1.3	5.0	10
S960	960	1.0, 1.025, 1.05, 1.1, 1.2, 1.3	6.9	10

Table 7: Class 1 and class 2 flange slenderness limits for mild steel hollow section

Ultimate strength/yield ratio	Class 1 limit considering rotation capacity criterion: $R > 3$		Class 2 limit considering resistance criterion: $M_u/M_{pl} > 1$	
f_u/f_y (-)	S355	S460	S355	S460
1.1	31.4	29.0	30.4	32.2
1.4	32.2	29.7	47.8	40.8

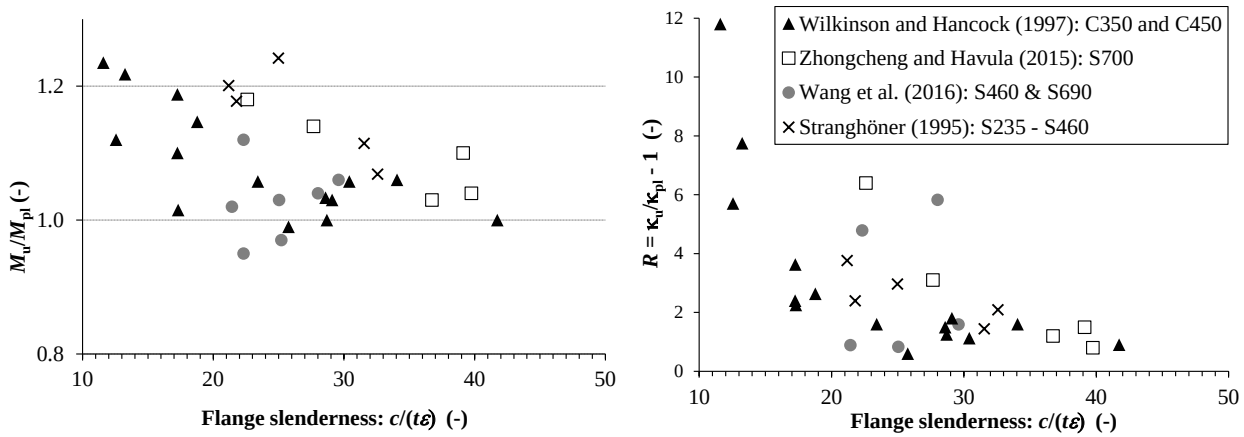

a) Non-dimensional bending resistance

b) Rotation capacity

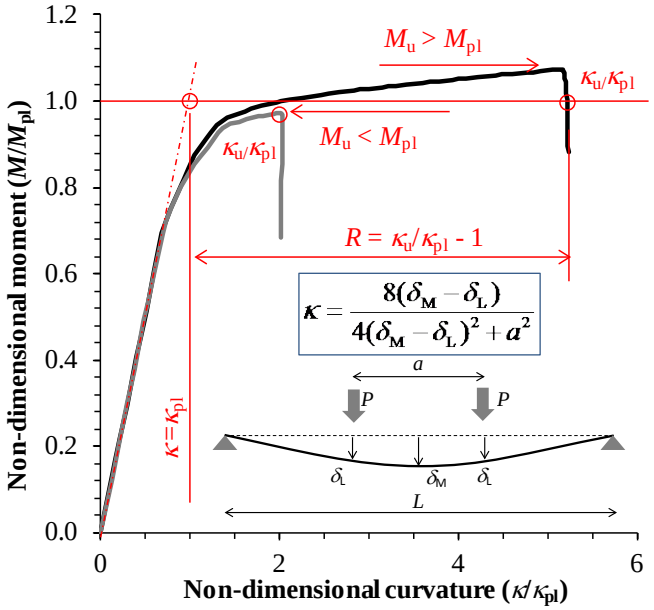

c) Typical non-dimensional moment-rotation curves

Figure 1. Experiment results of rectangular and square hollow section beams.

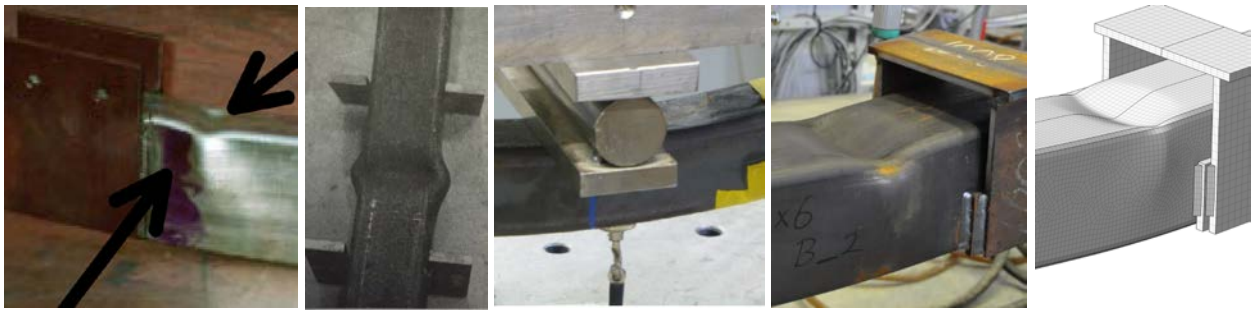

a) Wilkinson and Hancock b) Stranghöner c) Wang et al. d) Zhongcheng and Havula e) FEA validation

Figure 2. Local web and flange buckling near the loading section in bending experiments and FEA.

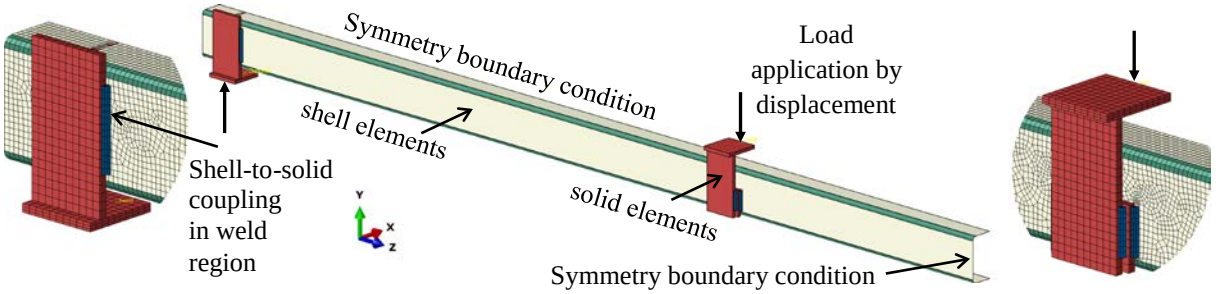

Figure 3: FE model of 4-point bending experiments.

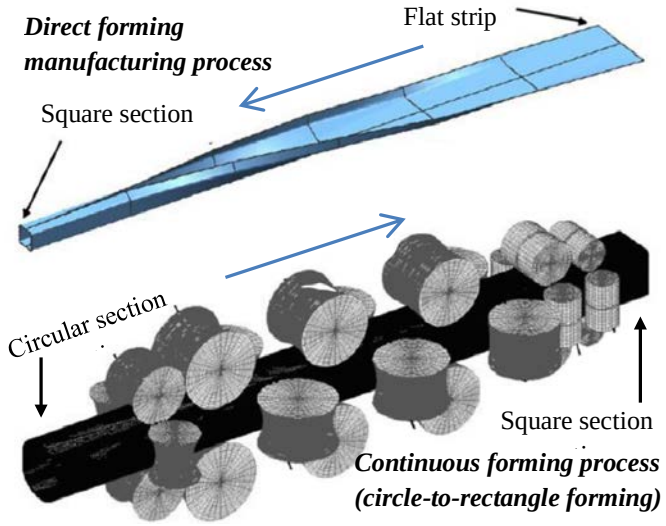

a) Forming processes (Li et al. 2009)

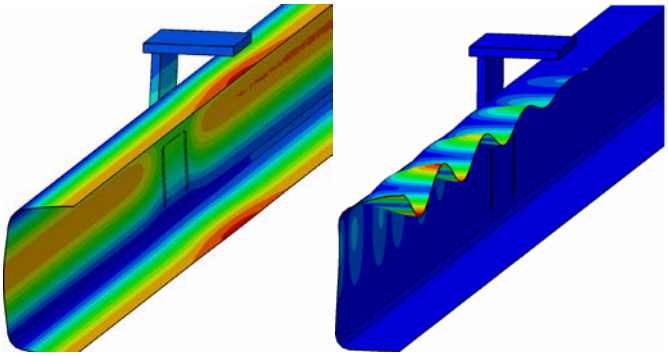

b) "bow-out" imperfections *c) Eigen-mode due to bending load*

Figure 4: Typical equivalent geometric imperfections used in nonlinear analysis.

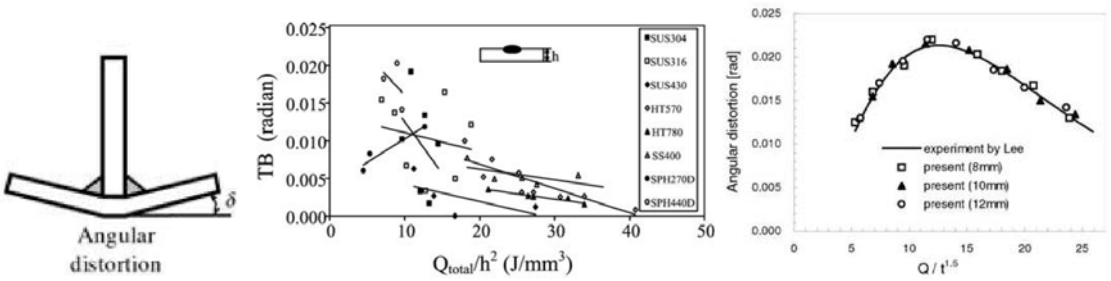

a Shape of distortion *b) bead-on-plate welds, Jang et al. (2002)* *c) fillet welds, Wang et al. (2009)*

Figure 5: Transverse bending (angular distortion) due to welding.

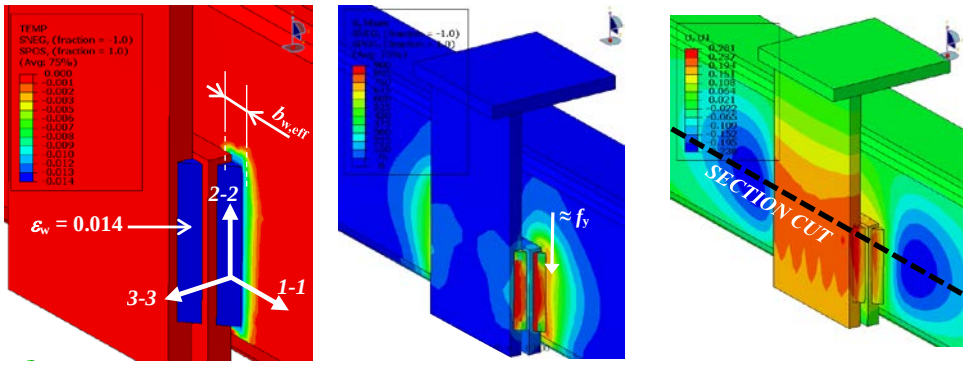

a) applied strains *b) residual stresses (von Mises)* *c) out of plane deformations*

Figure 6: Welding induced imperfections applied in FE model of RHS 140x140x6.

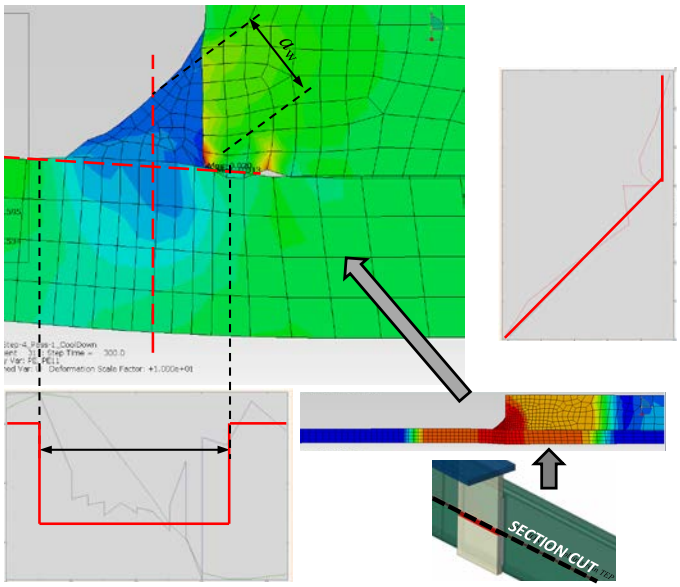

a) TEP analysis of fillet weld between the web and the loading plate

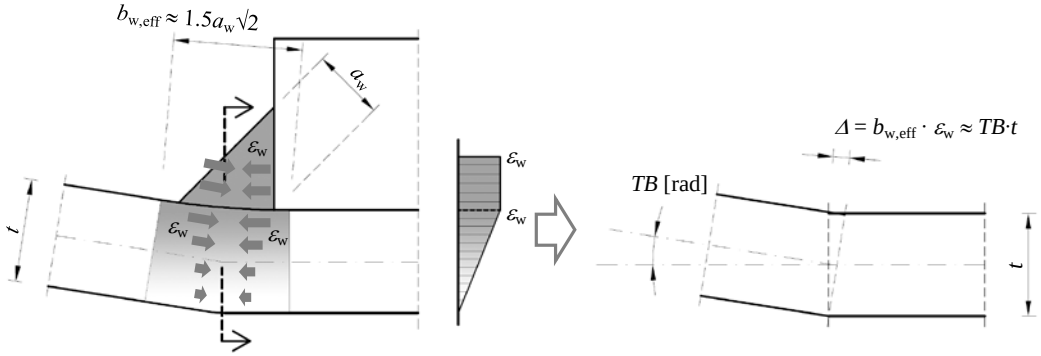

b) plastic strain distribution *c) strain vs. angular distortion TB*

Figure 7. Model of distribution of plastic strains induced by welding.

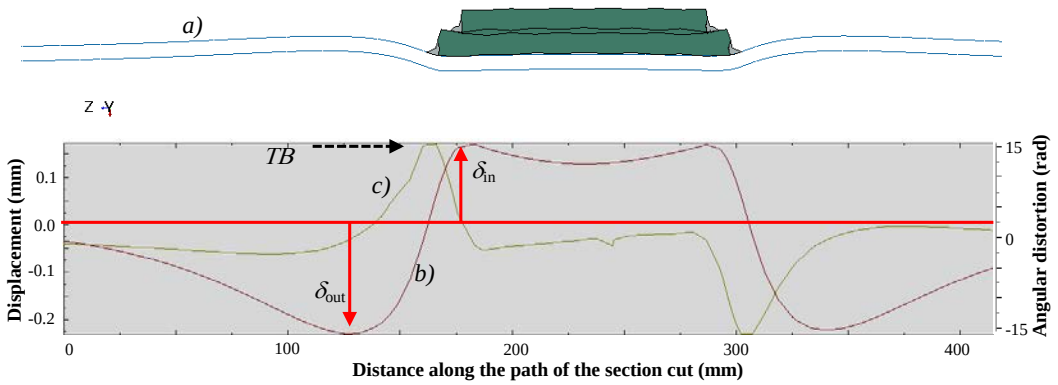

Figure 8: Out of plane deformation of the web in RHS 140x140x6: a) the deformed shape (scale x20); b) the deformation and c) the first derivative of the displacement (angular distortion)

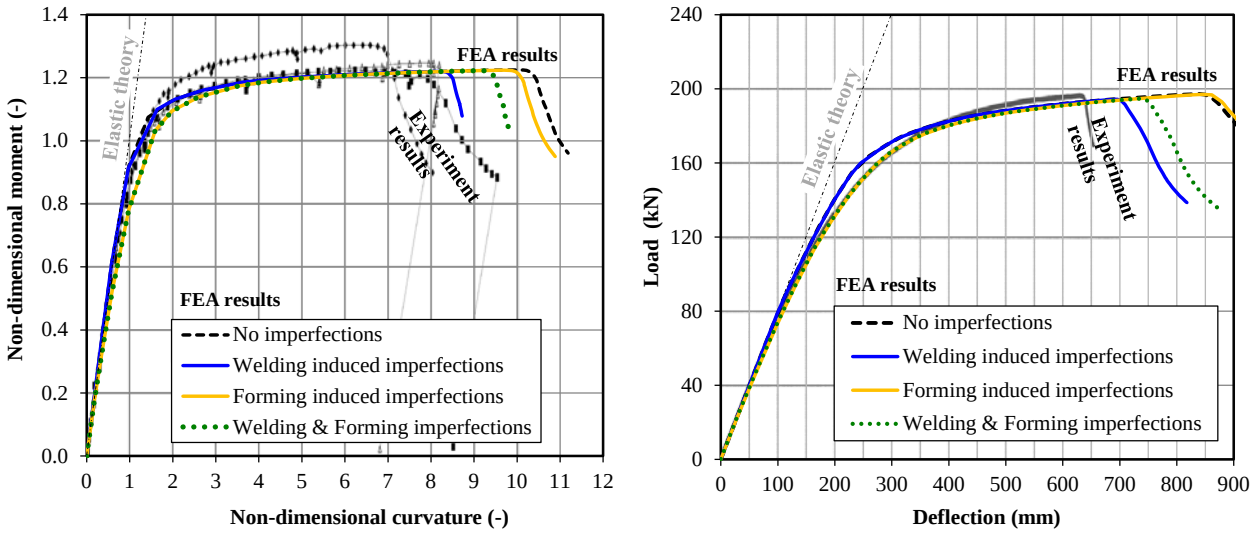

a) RHS 150x50x4 - Wilkinson and Hancock (1997) *b) SHS 150x150x8 - Zhongcheng and Havula (2015)*

Figure 9: Validation of imperfections in FEA vs. experiment results.

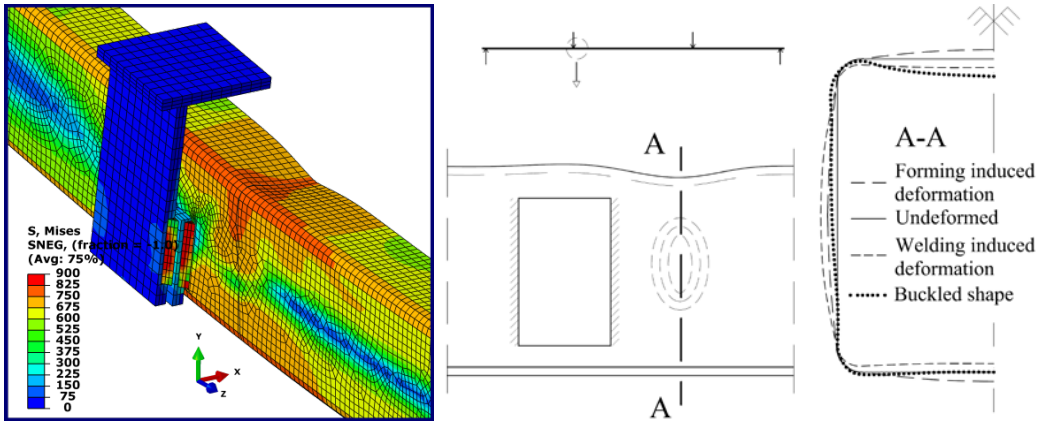

Figure 10: Diminishing effect of the forming induced imperfections on reduction of the rotation capacity.

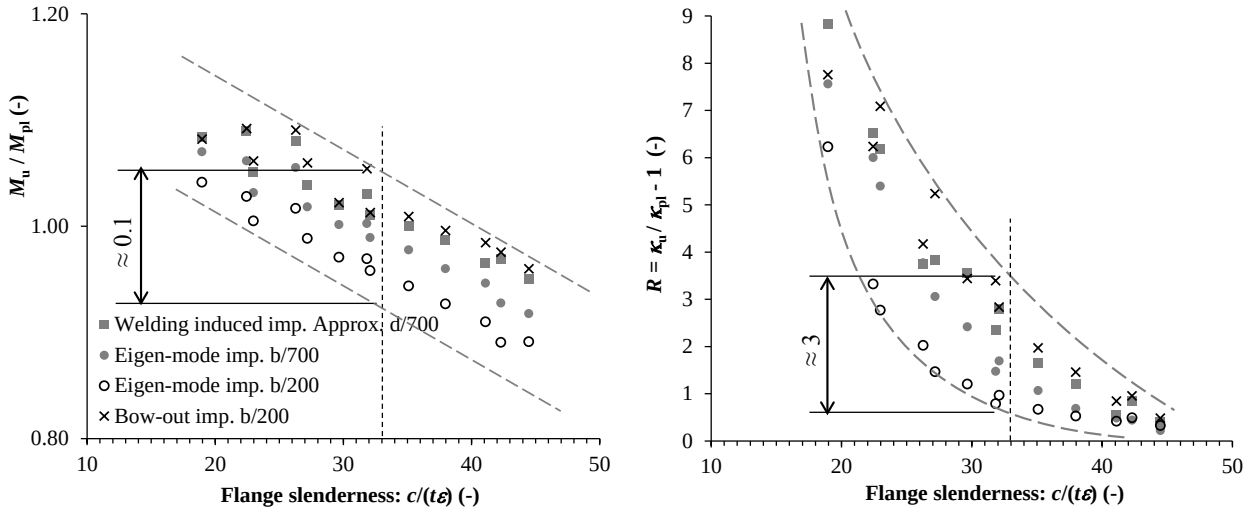

a) Non-dimensional bending resistance *b) Rotation capacity*

Figure 11: Influence of equivalent geometric imperfections vs. welding induced imperfections on cross section classification.

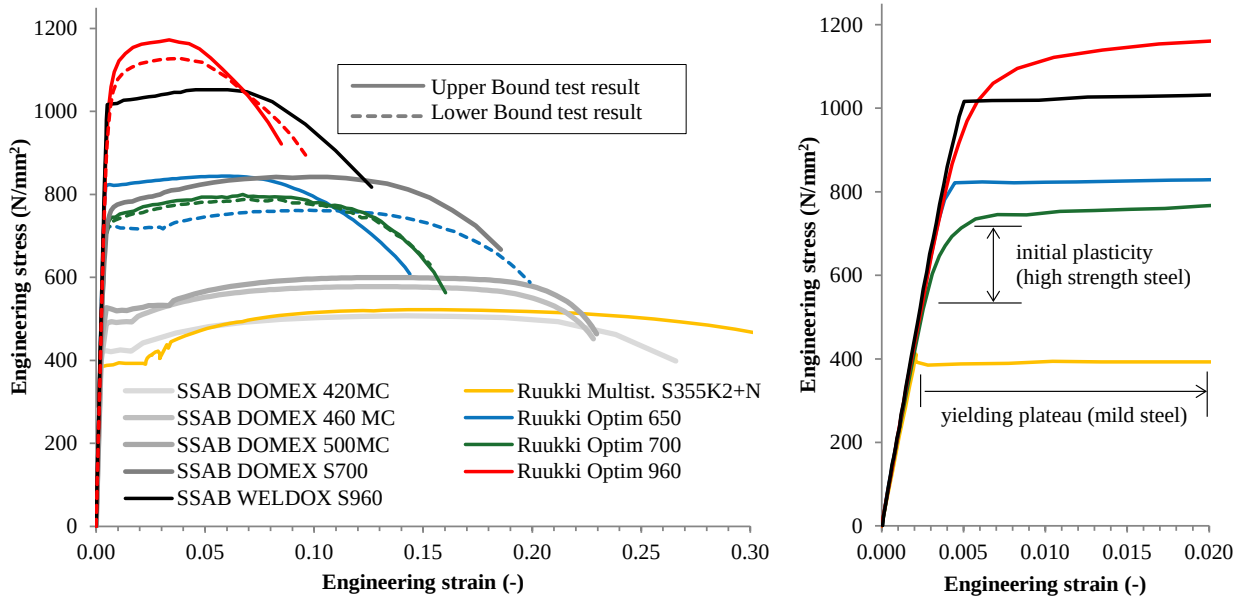

Figure 12: Results of tensile tests on various HSS and MS (RUOSTE, 2016)

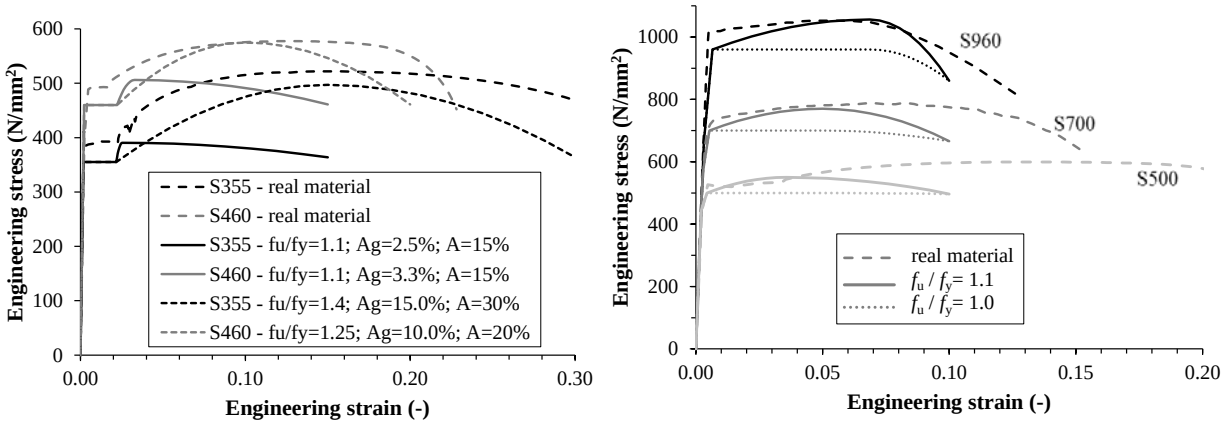

a) Mild-steel (MS) *b) High-strength steel (HSS)*

Figure 13: Materials used in the parametric study

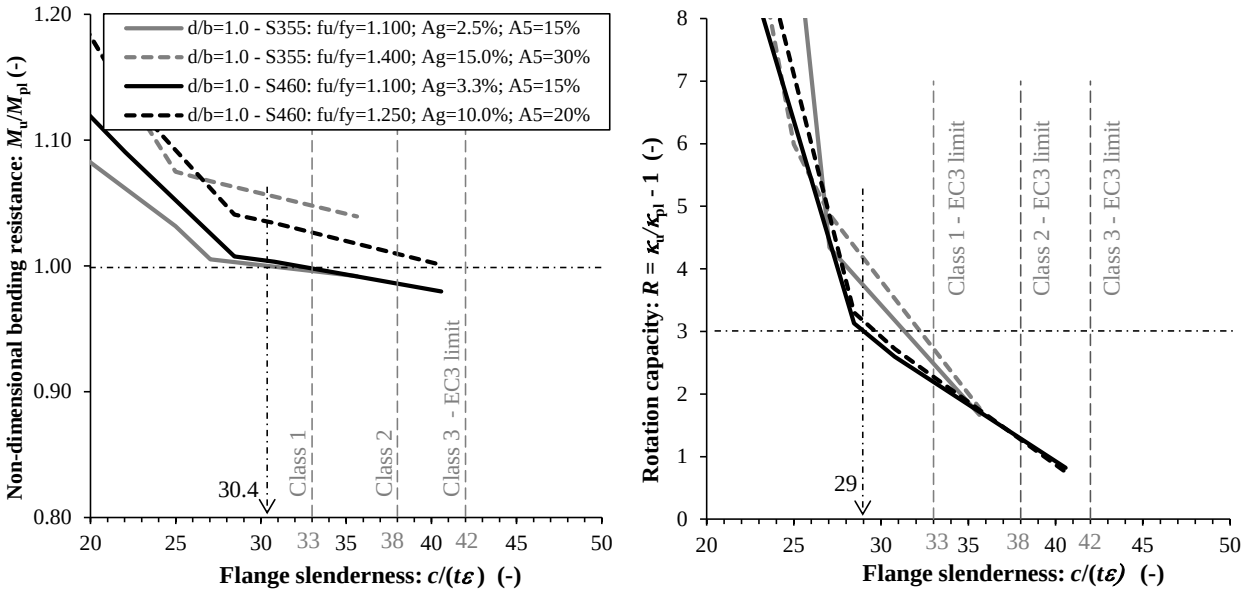

a) Non-dimensional moment *b) Rotation capacity*

Figure 14: Cross section class 1 and 2 limits for mild-steel beams - realistic vs. nominal material.

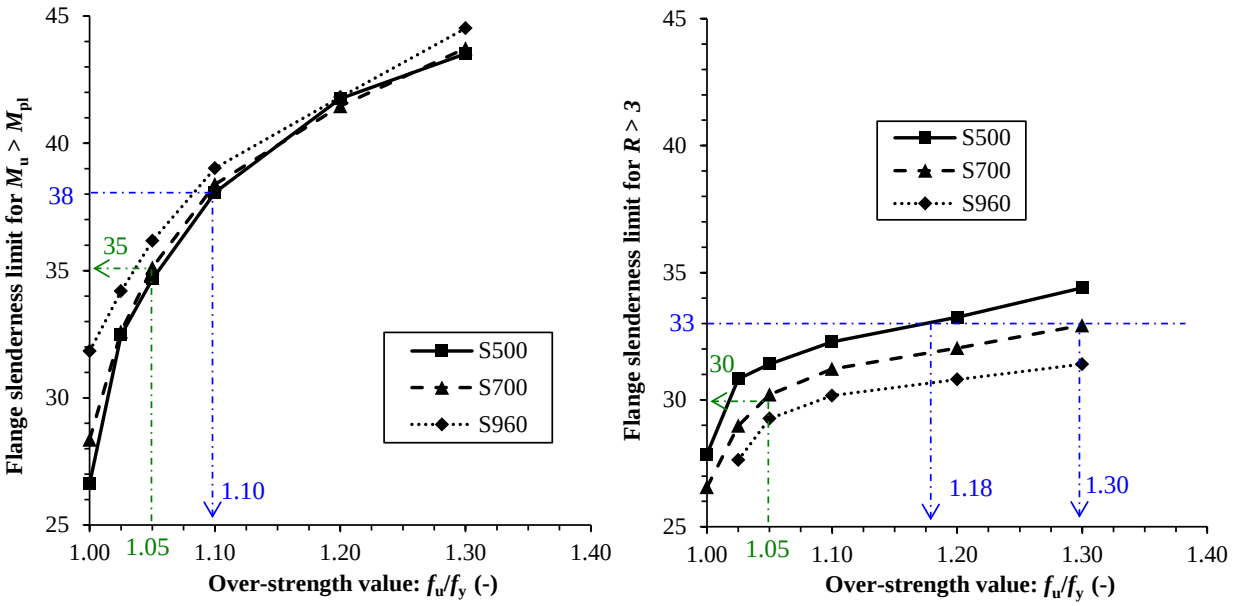

a) Resistance criterion – Class 2 *b) Rotation capacity criterion – Class 1*

Figure 15: Cross section class limits for high strength steel beams – influence of the ultimate-to-yield strength ratio.